NASA TECHNICAL NOTE

NASA TN D-3401

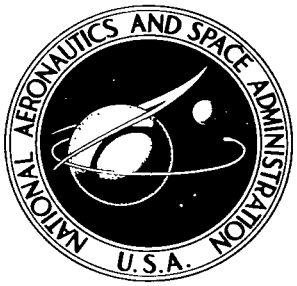

NASA TN D-3401

AERODYNAMIC CHARACTERISTICS OF RAKED-OFF CIRCULAR AND ELLIPTICAL CONES AT A MACH NUMBER OF 20 IN HELIUM

by John K. Molloy

Langley Research Center

Langley Station, Hampton, Va.

NATIONAL AERONAUTICS AND SPACE ADMINISTRATION • WASHINGTON, D. C. • APRIL 1966

AERODYNAMIC CHARACTERISTICS OF RAKED-OFF CIRCULAR AND ELLIPTICAL CONES AT A MACH NUMBER OF 20 IN HELIUM

By John K. Molloy

Langley Research Center
Langley Station, Hampton, Va.

NATIONAL AERONAUTICS AND SPACE ADMINISTRATION

For sale by the Clearinghouse for Federal Scientific and Technical Information
Springfield, Virginia 22151 – Price $2.00

AERODYNAMIC CHARACTERISTICS OF RAKED-OFF CIRCULAR AND ELLIPTICAL CONES AT A MACH NUMBER OF 20 IN HELIUM

By John K. Molloy
Langley Research Center

SUMMARY

An experimental investigation of the longitudinal and lateral directional aerodynamic characteristics of a new vehicular concept suitable for earth entry at hyperbolic speeds has been conducted in helium at a Mach number of approximately 20 and at Reynolds numbers ranging from 0.30×10^6 to 0.72×10^6. The configurations consisted of raked-off sharp circular cones and a raked-off sharp elliptical cone. In this investigation, the cone semivertex angles and rake-off angles ranged from 35° to 45° and from 51° to 68°, respectively; as a result, lift-drag ratios ranging from 0.40 to 0.80 were obtained at an angle of attack of 0°. The experimental aerodynamic characteristics were compared with the predictions of Newtonian theory. Newtonian theory underpredicted the longitudinal characteristics by not more than 10 percent for the raked-off circular cones and by approximately 16 percent for the raked-off elliptical cone. Newtonian predictions of the lift-drag ratios were slightly higher for all the configurations. The experimental values and the theoretical predictions of the lateral-directional characteristics were in very good agreement. Excellent agreement existed between the Newtonian and the experimental stability derivatives. Center-of-gravity locations required for the raked-off circular cones to be trimmed and statically stable in the directional mode at an angle of attack and angle of sideslip of 0° tended to become unrealistic as the rake-off angle was decreased. The raked-off elliptical cone, in which the cone half-angle measured in the horizontal plane is greater than the cone half-angle measured in the vertical plane, tended to alleviate the aforementioned directional instabilities.

INTRODUCTION

A new concept of a vehicle capable of earth reentry at hyperbolic speeds has been proposed in reference 1. These configurations, while trimmed at an angle of attack of 0°, are capable of minimizing the combined radiative and convective heating at hyperbolic speeds and also of producing hypersonic lift-drag ratios, which are desirable. (See ref. 2.) In the preliminary investigations, two types of configurations are being considered. They consist of a right circular cone forebody raked off to produce an elliptical interface which

is mated to an elliptical cone afterbody, and an elliptical cone forebody raked off to produce a circular interface which is mated to a right circular cone afterbody. A detailed theoretical study of the aerodynamic characteristics of both types of forebodies was performed in reference 3.

The purpose of this paper is to provide, for several of these forebody shapes, experimental hypersonic stability characteristics for comparison with the theoretical Newtonian values. In this investigation, five raked-off right circular cones and one raked-off elliptical cone were tested. For the raked-off right circular cones, the cone angle was held constant and the rake-off angle varied and then the rake-off angle was held constant and the cone angle varied. The cone semivertex angles and rake-off angles varied from 35° to 45° and from 51° to 68°, respectively; as a result, lift-drag ratios ranging from 0.40 to 0.80 at $\alpha = 0^\circ$ were obtained. It should also be noted that for entry velocities of approximately 65,000 feet per second (19812 m/s) and this range of cone angles, both the radiative and convective heating are minimized. (See ref. 1.)

The tests were performed in helium at a Mach number of approximately 20 and at Reynolds numbers ranging from 0.30×10^6 to 0.72×10^6 based on characteristic length D. The aerodynamic characteristics are presented over an angle-of-attack range from -4° to 10° at 0° sideslip and over an angle-of-sideslip range from -6° to 5° at an angle of attack of 0°.

SYMBOLS

D characteristic length for yawing moment, rolling moment, and pitching moment (see fig. 1)

S reference area, $\frac{\pi D^2}{4}$

C_A axial-force coefficient, $\frac{\text{Axial force}}{q_\infty S}$

C_D drag coefficient, $\frac{\text{Drag}}{q_\infty S}$

C_L lift coefficient, $\frac{\text{Lift}}{q_\infty S}$

C_l rolling-moment coefficient (about longitudinal axis), $\frac{\text{Rolling moment}}{q_\infty SD}$

C_N normal-force coefficient, $\frac{\text{Normal force}}{q_\infty S}$

C_n yawing-moment coefficient (referenced to nose), $\frac{\text{Yawing moment}}{q_\infty SD}$

$C_{A_\alpha} = \frac{\partial C_A}{\partial \alpha}$ per degree

$C_{N_\alpha} = \frac{\partial C_N}{\partial \alpha}$ per degree

$C_{l_\beta} = \frac{\partial C_l}{\partial \beta}$ per degree

$C_{n_\beta} = \frac{\partial C_n}{\partial \beta}$ per degree

C_Y side-force coefficient, $\frac{\text{Side force}}{q_\infty S}$

$C_{Y_\beta} = \frac{\partial C_Y}{\partial \beta}$ per degree

C_m pitching-moment coefficient (referenced to nose), $\frac{\text{Pitching moment}}{q_\infty SD}$

$C_{m_\alpha} = \frac{\partial C_m}{\partial \alpha}$ per degree

L/D lift-drag ratio

q_∞ free-stream dynamic pressure

M_∞ free-stream Mach number

R_D free-stream Reynolds number based on D

α angle of attack, degree

β angle of sideslip, degree

θ cone half-angle, degree

θ_{xy} cone half-angle measured in horizontal plane, degree

θ_{xz} cone half-angle measured in vertical plane, degree

δ rake-off angle, degree

x,y,z distance along X-, Y-, and Z-axis, respectively

MODELS AND APPARATUS

The models were constructed of aluminum and were internally bored to receive a six-component strain-gage balance, which was used to measure the forces and moments. A sketch of the configurations and model balance orientations are shown in figure 1 along with a table listing the important physical dimensions. As indicated in the sketch of the raked-off right circular cones (fig. 1(a)), the right circular cone with a semivertex angle of 35° had rake-off angles of 68°, 59°, and 51°, and the 40° and 45° cones had rake-off angles of 59° and 58.65°, respectively. Figure 1(b) illustrates the raked-off 45° cone with a representative afterbody, which consisted of an elliptical cone. The elliptical cone, shown in figure 1(c), had a cone angle of 35° in the vertical plane, a cone angle of 42° in the horizontal plane, and a rake-off angle of 59°. In figure 1(d), a sketch of the model-balance orientation is shown. Some photographs of the models are shown in figure 2.

The tests were conducted in the Langley 22-inch helium tunnel with the $M_\infty = 22$ contoured nozzle installed. A sketch of the tunnel with the contoured nozzle installed is shown in figure 3. A detailed description of this facility along with the results of Mach number and flow angularity surveys conducted in this nozzle are contained in the appendix of reference 4.

TESTS AND ACCURACY

The models were mounted on a sting-supported strain-gage balance. Angles of attack and sideslip were measured by using a small prism mounted in the shielded rear region of the model to reflect the light from a point source on to photoelectric cells, which were set at calibrated intervals. The models were continuously rotated in pitch or sideslip and as the reflected light swept past each cell, an electrical relay was energized and caused a high-speed digital recorder to sample and record the strain-gage outputs on magnetic tape.

The average test Mach number and Reynolds number for the longitudinal stability characteristics was 20.2 and 0.36×10^6 per inch (per 2.54 cm), respectively. The average test Mach number and Reynolds number for the lateral data were 19.1 and 0.20×10^6 per inch (per 2.54 cm), respectively.

The maximum uncertainties in the force and moment coefficients as determined from a static calibration of the balance are as follows:

	C_N	C_A	C_m	C_l	C_n	C_Y
Models 1 and 2	±0.05	±0.01	±0.01	±0.003	±0.007	±0.01
Models 3 and 4	±.08	±.02	±.03	±.005	±.010	±.008
Model 5	±.05	±.05	±.01	±.016	±.03	±.025
Model 6	±.02	±.05	±.01	±.003	±.007	±.01

Angles of attack and sideslip were known to $\pm 0.1^{\circ}$. Two sets of data were taken for each test, inasmuch as the reflected light from the prism swept past the photoelectric cells twice (in opposite directions) during each run. The difference between the two sets of data was within the quoted accuracy of the balance. Data presented in this report represent an average of the two sets of data. The models were set at 0° in roll and sideslip and rotated continuously in angle of attack to obtain the longitudinal characteristics. In order to obtain the lateral-directional characteristics, the models were set at 0° in roll and angle of attack and rotated continuously in sideslip. Model base pressures were not measured and therefore the coefficients are not adjusted to a condition where free-stream static pressure acts on the base of the models.

RESULTS AND DISCUSSION

The theoretical Newtonian aerodynamic characteristics presented in this paper were calculated by the methods contained in reference 3. A maximum stagnation-point pressure coefficient of 2.0 was used for the theoretical Newtonian solutions. Exact inviscid cone solutions are also presented for the aerodynamic characteristics of the raked-off circular cones at $\alpha = 0^{\circ}$.

In figures 4 and 5 the experimental and theoretical longitudinal and lateral-directional aerodynamic characteristics are presented for a 35° right circular cone having rake-off angles δ of 68°, 59°, and 51°. As would be expected, a decrease in rake angle is seen to produce an increase in the values of lift, drag, and the lift-drag ratio, a more negative value of pitching moment and side force, and a more positive value of yawing moment. It should be noted that for the particular reference moment location used, the rolling moment is zero for these configurations. It may be of interest to note that these same trends occur when the projected frontal area is used as a reference area instead of $\frac{\pi D^2}{4}$. However, when the projected frontal area is used as a reference area, smaller changes in C_L and C_D are to be expected with changes in δ, although the large variations in L/D with δ remain unchanged. It can be seen from these figures that fair agreement exists between the Newtonian and the experimental longitudinal characteristics (the theory underpredicting the experimental values by approximately 10 percent for the worst case). Newtonian predictions of the lift-drag ratios for the raked-off circular cone were usually about 4 or 5 percent higher than the experimental values at $\alpha = 0^{\circ}$. The Newtonian predictions of the lateral-directional characteristics are in very good agreement with the experimental values.

The solid symbols in figure 4 represent theoretical predictions (at $\alpha = 0^{\circ}$) of the aerodynamic characteristics obtained by using a pressure coefficient determined by exact inviscid cone solutions. These pressure coefficients were obtained from reference 5. It can be seen in figure 4 that the theoretical aerodynamic characteristics obtained by this method agree with the experimental values much better than the Newtonian predictions.

It appeared from the theoretical design analysis that cone angles in the range of 35° to 45° would meet the necessary design requirements; these

requirements included minimum radiative and convective heating at hyperbolic speeds and adequate L/D values to meet reentry-corridor and trajectory-control requirements.

Therefore, in order to find the aerodynamic effect of cone angle, cones having semivertex angles of 35°, 40°, and 45° were investigated. The rake-off angle was held essentially constant for these configurations, the angle being 59° for the 35° and 40° cones and 58.65° for the 45° cone.

A comparison of the experimental and theoretical longitudinal aerodynamic characteristics is presented in figure 6. The Newtonian theory underpredicts the experimental values by approximately 10 percent for the worst case, which is the $\theta = 45°, \delta = 58.65°$ configuration.

It should be noted that although the lift and drag increase with increasing cone angle, the lift-drag ratio remains approximately constant at $\alpha = 0°$. The raked-off 45° cone has a slightly higher L/D because of the slight difference in rake angle (L/D increases with decrease in rake angle). However, for angles different from zero the lift-drag ratios are dependent on the cone angle. The use of projected frontal area as a reference area instead of $\frac{\pi D^2}{4}$ produces no change in the trends shown in figure 6.

In order to assure that the presence of an afterbody would not have significant effects on the stability characteristics, the raked 45° cone was tested with a representative afterbody, as shown in figure 1(b). The afterbody consisted of a right elliptical cone mated to the forebody. The aerodynamic characteristics of this configuration are contained in figure 6 and are denoted by the flagged symbols. It can be seen from this figure that the effect of having an afterbody on this particular configuration for this angle-of-attack range was negligible.

The experimental and the theoretical predictions of the aerodynamic characteristics for the raked-off elliptical cone are presented in figure 7. The slopes of the experimental and theoretical longitudinal characteristics are in good agreement; however, the Newtonian theory underpredicts the experimental values by approximately 15 percent. Since the experimental values of C_L and C_D are underpredicted by approximately the same amount, the agreement between the experimental L/D values and the theoretical values is excellent. It should be noted that although the raked-off elliptical cone had a higher lift and drag than the $\theta = 35°, \delta = 59°$ raked-off circular cone, the value of the lift-drag ratio at $\alpha = 0°$ was approximately the same. The directional stability results are presented in figure 7(c). It is evident from this figure that the agreement between the experimental values and the theoretical predictions is very good. It should also be noted that the agreement between theory and experiment is much better for the directional characteristics than for the longitudinal characteristics; this result was also obtained for the case of the raked-off circular cones. This result was also found in reference 6 which contains a similar investigation at a lower Mach number. In figure 8, it is shown that excellent agreement exists between the Newtonian and experimental values of

the aerodynamic stability derivatives at $\alpha = \beta = 0^\circ$ for all the configurations investigated.

In order for these configurations to exhibit the minimum heat-transfer qualities for which they were chosen, it is necessary that they glide at an angle of attack of 0°. Therefore it is necessary that the configurations be statically stable and trimmed at $\alpha = \beta = 0^\circ$.

Figure 9 shows, for each of the configurations investigated, the loci of center-of-gravity positions for trim at $\alpha = \beta = 0^\circ$ and the limiting center-of-gravity positions (determined theoretically and experimentally) that will permit trimmed statically stable flight in the longitudinal or directional mode. That is, neutral stability exists at the indicated locations and unstable conditions exist when the center of gravity is located rearward of the indicated locations. The appendix contains the equations used to determine these limiting center-of-gravity locations for trimmed stable flight at $\alpha = \beta = 0^\circ$. It should be noted that within the angle-of-attack range for which these configurations were tested, all the force and moment coefficients vary linearly with α and β. As a consequence of this linearity, the longitudinal and directional center-of-gravity positions noted in figure 9 will make $C_m = C_{m_\alpha} = 0$ and $C_n = C_{n_\beta} = 0$, respectively, at any α or β within the linear range. The differences shown in figure 9 between the center-of-gravity positions determined experimentally and theoretically are due mainly to slight differences in the aerodynamic derivatives. It can be seen from figures 9(a) and 9(b) that for raked-off circular cones, the necessary center-of-gravity location for trimmed stable flight is dictated by the directional stability limit, as the center of gravity must be located ahead of the most forward of the two locations given and must lie on the dashed line shown, along which trim at $\alpha = 0^\circ$ is obtained. It is also shown in figure 9(a) that as the rake-off angle is decreased and, therefore, L/D is increased, the center-of-gravity requirements tend to become unrealistic. That is, it would be very difficult, if not impossible, to have the weight of the capsule distributed in such a way that the center of gravity would act through a point located so near the front lower face of the model. Since the 40° and 45° raked-off circular cones were not tested for directional stability, only the theoretical predictions of the limiting center-of-gravity locations for directional stability are shown. (However, it can be seen from figure 9(a) that the experimental and theoretical predictions of the limiting center-of-gravity locations for directional stability are in good agreement.) From a comparison of the limiting center-of-gravity locations of the 35°, 40°, and 45° right circular cones raked off at 59°, it can be seen that increasing the bluntness of the raked-off circular cones tends to give more realistic center-of-gravity positions for directional stability.

Another means of obtaining more realistic center-of-gravity locations for directional stability is a raked-off elliptical cone, in which the cone half-angle measured in the horizontal plane is always greater than the cone half-angle measured in the vertical plane. In order that a comparison could be drawn as to how much the directional stability was improved, two of the geometric properties of one of the raked-off circular cones were chosen (that is, $\theta_{xz} = 35^\circ, \delta = 59^\circ$) and then θ_{xy} was chosen so that when the elliptical cone

was raked off at 59°, the mating part of the elliptical forebody was circular. (See fig. 1(c).) The improvement that this configuration produced in the limiting center-of-gravity location for directional stability may be seen in figure 9(a).

CONCLUSIONS

An experimental investigation of the static longitudinal and lateral directional characteristics of raked-off right circular cones, and a raked-off elliptical cone has been conducted in helium at a Mach number of approximately 20. A comparison of the experimental results with the theoretical Newtonian predictions showed the following:

1. The Newtonian theory underpredicted the longitudinal characteristics by not more than 10 percent for the raked-off circular cones and by approximately 15 percent for the raked-off elliptical cone.

2. Near an angle of attack of 0°, the Newtonian predictions of the lift-drag ratios were about 5 percent higher than the experimental values.

3. The Newtonian estimates of the lateral directional characteristics were in very good agreement with the experimental values for both the raked-off circular cones and the raked-off elliptical cone.

4. Agreement between the experimental and Newtonian stability derivatives at an angle of attack and angle of sideslip of 0° was excellent in all cases.

5. The center-of-gravity locations that would be required for some of the raked-off circular cones to be trimmed and statically stable in the directional mode at an angle of attack and angle of sideslip of 0° were unrealistic. The raked-off elliptical cone tended to alleviate this situation.

Langley Research Center,
National Aeronautics and Space Administration,
Langley Station, Hampton, Va., January 14, 1966.

APPENDIX

EQUATIONS FOR LIMITING CENTER-OF-GRAVITY LOCATIONS

The center-of-gravity location that will permit the configuration to be trimmed and also to have neutral static longitudinal stability at $\alpha = \beta = 0^\circ$ was determined by requiring that $C_m = \frac{\partial C_m}{\partial \alpha} = 0$ about this point. These conditions lead to the following equations:

$$C_N \frac{x}{D} - C_A \frac{z}{D} + C_m = 0 \tag{1}$$

$$C_{N_\alpha} \frac{x}{D} - C_{A_\alpha} \frac{z}{D} + C_{m_\alpha} = 0 \tag{2}$$

where C_m is the moment about some arbitrary known point. The simultaneous solution of these equations yields the following equation for determining x/D and z/D, which are the dimensionless coordinates for the minimum required center-of-gravity position for these conditions:

$$\frac{x}{D} = \frac{C_m C_{A_\alpha} - C_A C_{m_\alpha}}{C_A C_{N_\alpha} - C_N C_{A_\alpha}} \tag{3}$$

$$\frac{z}{D} = \frac{C_m C_{N_\alpha} - C_N C_{m_\alpha}}{C_A C_{N_\alpha} - C_N C_{A_\alpha}} \tag{4}$$

where x and z are measured from the point about which the pitching moment C_m is referenced. When C_N, C_A, and C_m are linear with α, the values of x/D and z/D are independent of α.

The center-of-gravity location that will permit the configuration to be trimmed and also to have neutral static directional stability at $\alpha = \beta = 0^\circ$ was determined by requiring that $C_n = 0$ about this point and that $\frac{\partial C_n}{\partial \beta} = 0$. Since the configuration is symmetric in the X,Z plane, $C_n = 0$ at $\beta = 0^\circ$ and $\frac{\partial C_n}{\partial \beta} = 0$ at an x/D location given by $\frac{C_{n_\beta}}{C_{Y_\beta}}$. It should be noted that $\frac{\partial C_n}{\partial \beta} = 0$ at any z location in a plane parallel to the Y,Z plane which passes through the x location given by $\frac{C_{n_\beta}}{C_{Y_\beta}}$. If the curves for the variations of C_Y, C_A,

and C_n with β are linear, the center-of-gravity location required to have the configuration trimmed and directionally stable at an angle of attack and angle of sideslip of 0° will be independent of β.

REFERENCES

1. Anon.: Preliminary Design of a Mars-Mission Earth Reentry Module. 4-57-63-2 (Contract NAS 9-1702), Lockheed Missiles & Space Co., Jan. 7, 1964.

2. Love, E. S.; and Pritchard, E. B.: A Look at Manned Entry at Circular to Hyperbolic Velocities. Paper presented at AIAA Second Manned Space Flight Symposium, Apr. 1963.

3. Mayo, Edward E.; Lamb, Robert H.; and Romere, Paul O.: Newtonian Aerodynamics for Blunted Raked-Off Circular Cones and Raked-Off Elliptical Cones. NASA TN D-2624, 1965.

4. Arrington, James P.; Joiner, Roy C., Jr.; and Henderson, Arthur, Jr.: Longitudinal Characteristics of Several Configurations at Hypersonic Mach Numbers in Conical and Contoured Nozzles. NASA TN D-2489, 1964.

5. Henderson, Arthur, Jr.; and Braswell, Dorothy O.: Charts for Conical and Two-Dimensional Oblique-Shock Flow Parameters in Helium at Mach Numbers From About 1 to 100. NASA TN D-819, 1961.

6. Bernot, Peter T.: Static Stability Characteristics of Several Raked-off Circular and Elliptical Cones at Mach 6.7. NASA TN D-3053, 1965.

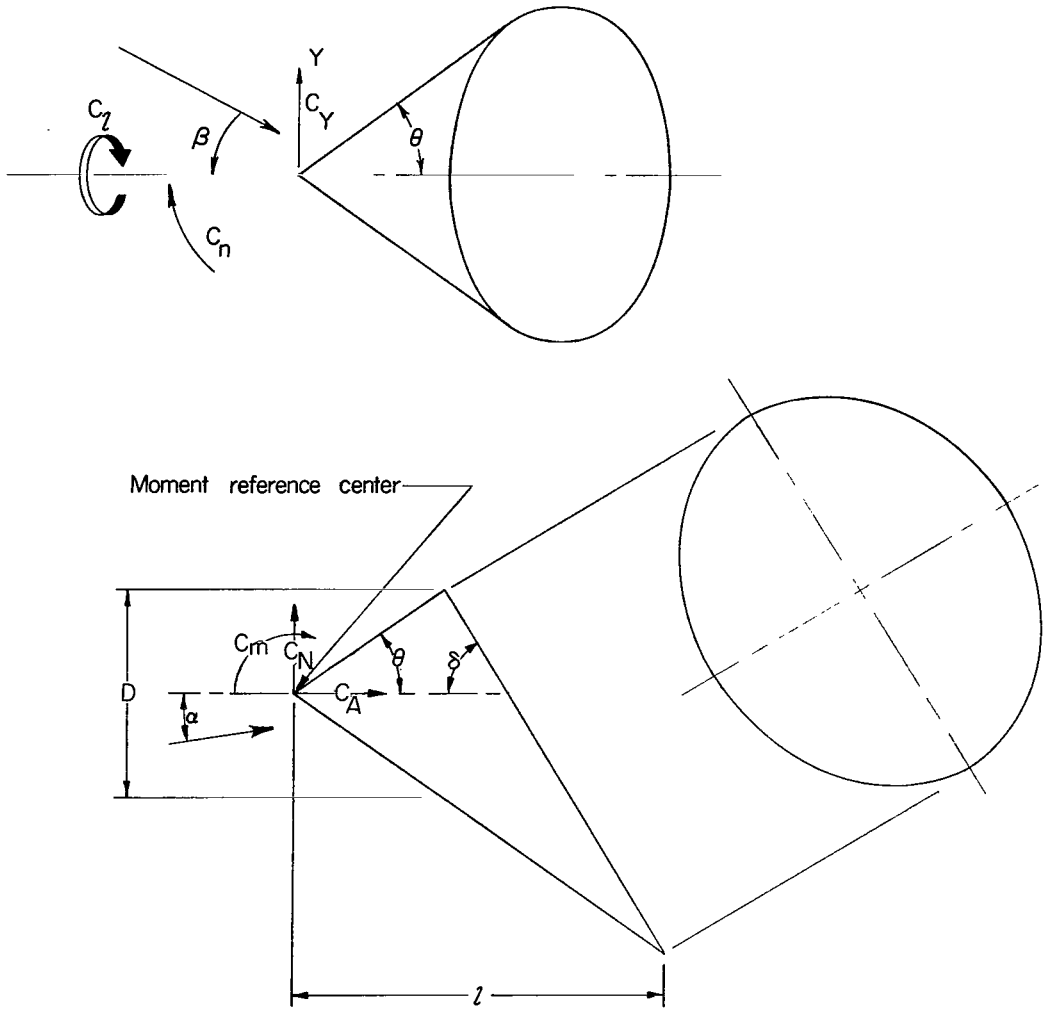

Model	θ, deg	δ, deg	D, cm	l, cm
1	35	68	5.08	6.48
2	35	59	5.08	8.89
3	35	51	3.81	9.86
4	40	59	3.81	6.88
5	45	58.65	3.048	6.27

(a) Raked-off circular cone.

Figure 1.- Sketch of models.

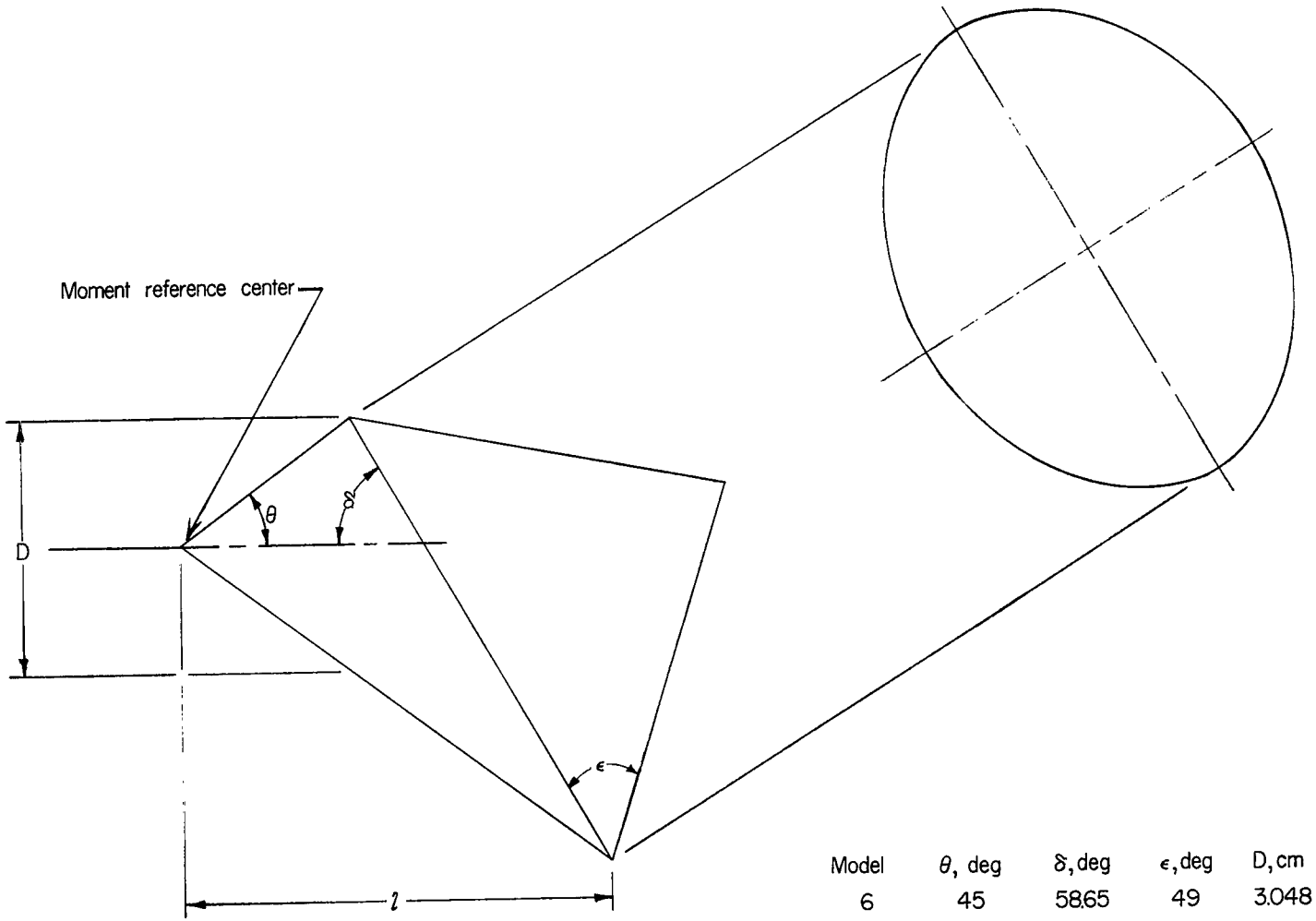

Model	θ, deg	δ, deg	ε, deg	D, cm	l, cm
6	45	58.65	49	3.048	6.27

(b) Raked-off circular cone with afterbody.

Figure 1.- Continued.

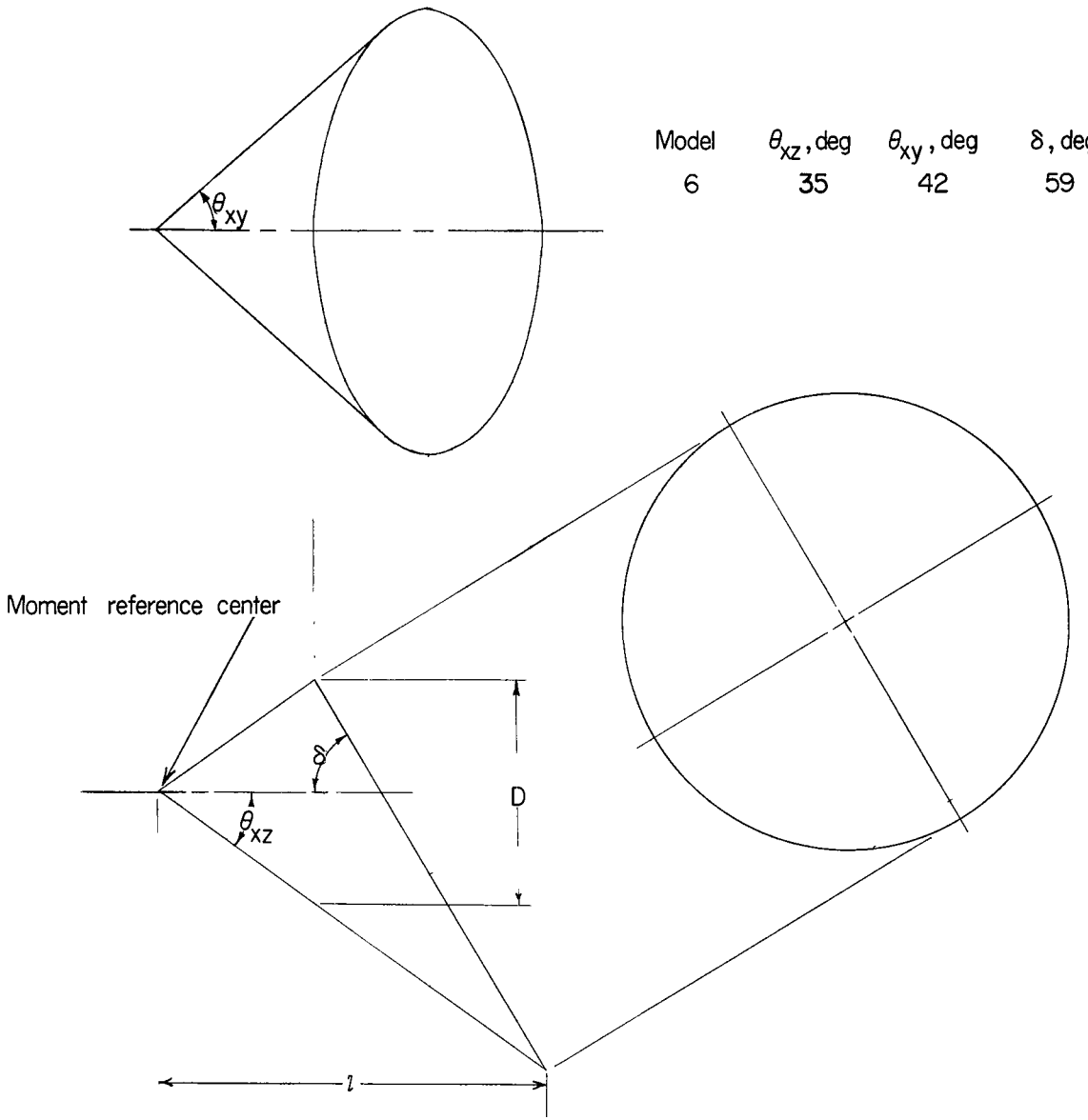

Model	θ_{xz}, deg	θ_{xy}, deg	δ, deg	D, cm	l, cm
6	35	42	59	5.08	8.89

(c) Raked-off elliptical cone.

Figure 1.- Continued.

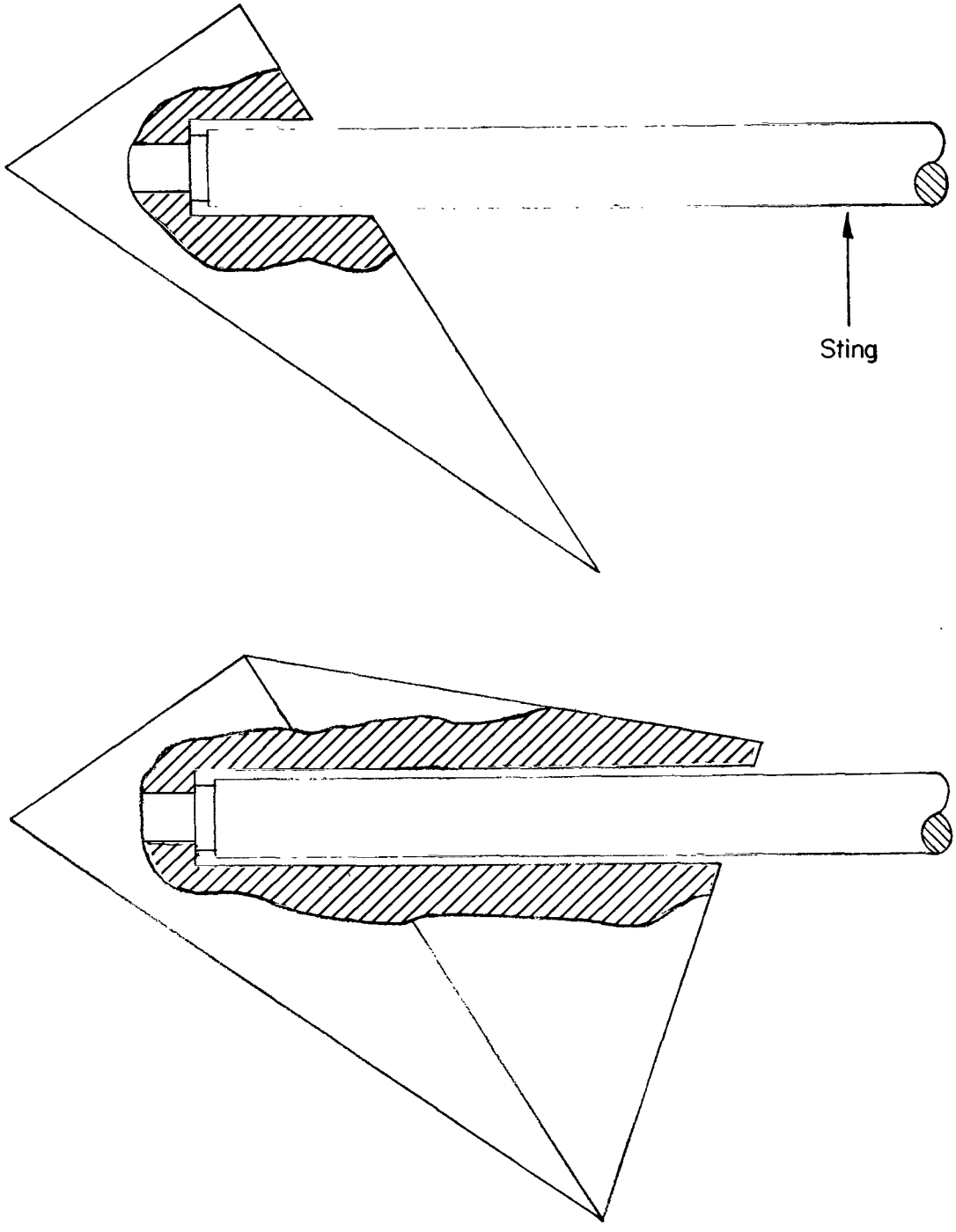

(d) Model-balance orientations.

Figure 1.- Concluded.

(a) Raked-off circular cone. L-65-8002

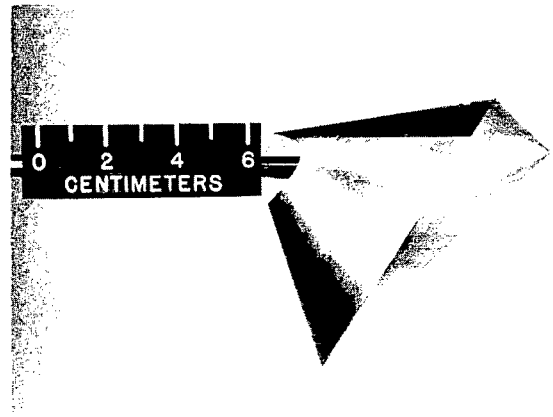

(b) Raked-off circular cone with afterbody. L-65-8004

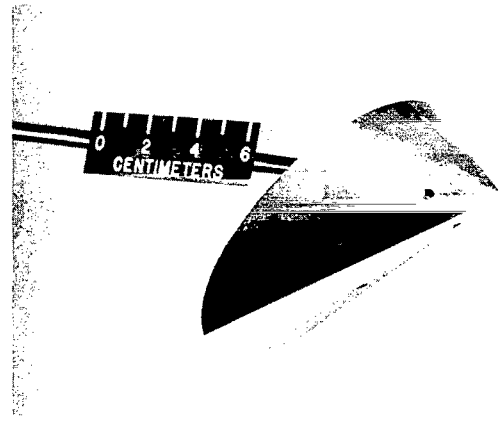

(c) Raked-off elliptical cone. L-65-8006

Figure 2.- Photographs of test models.

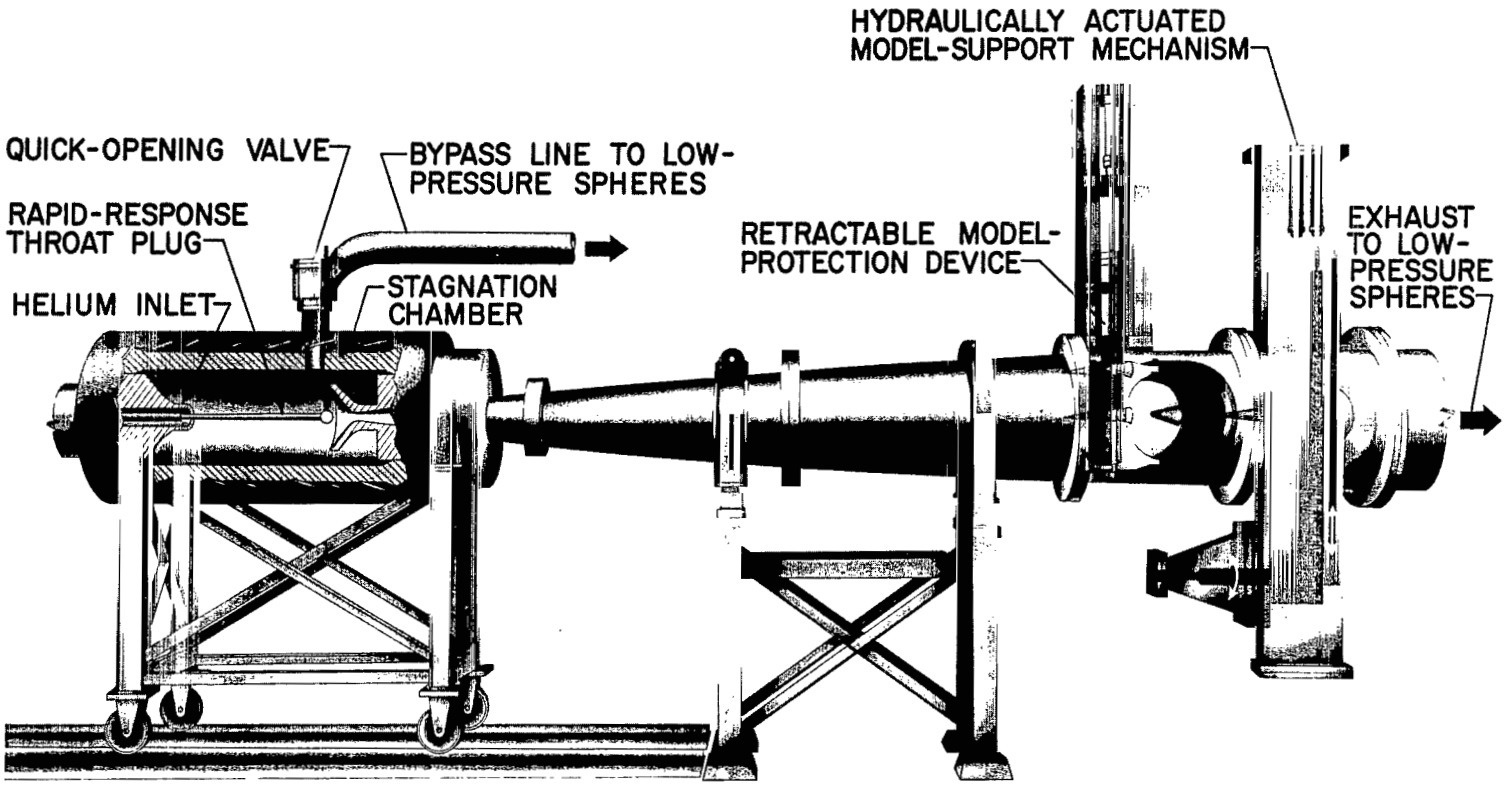

Figure 3.- Langley 22-inch helium tunnel.

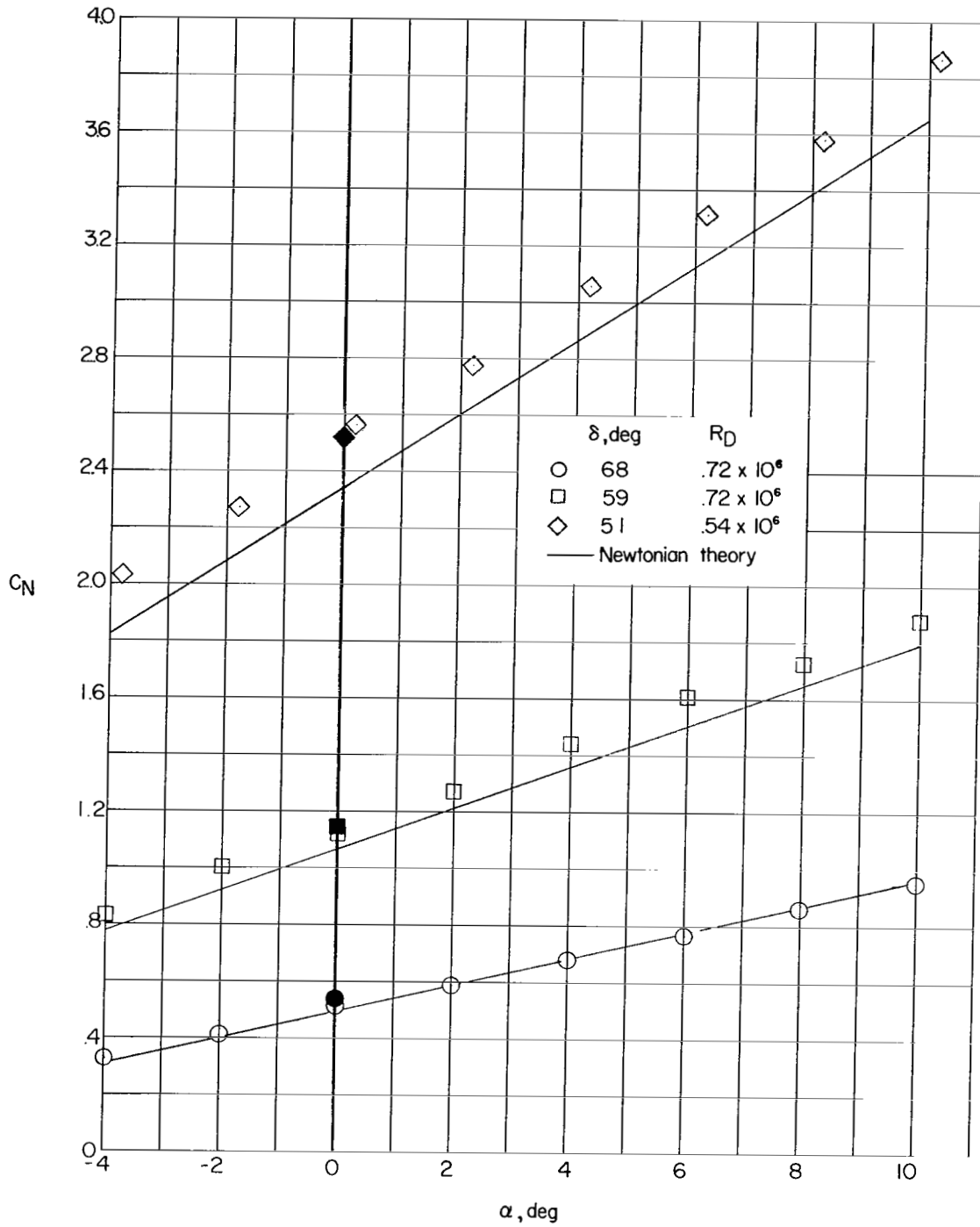

(a) Variation of C_N with α.

Figure 4.- Effect of rake-off angle on the longitudinal characteristics of circular cones. $\theta_{xz} = 35^0$; $M_\infty = 20.2$. Solid symbols represent exact cone solutions.

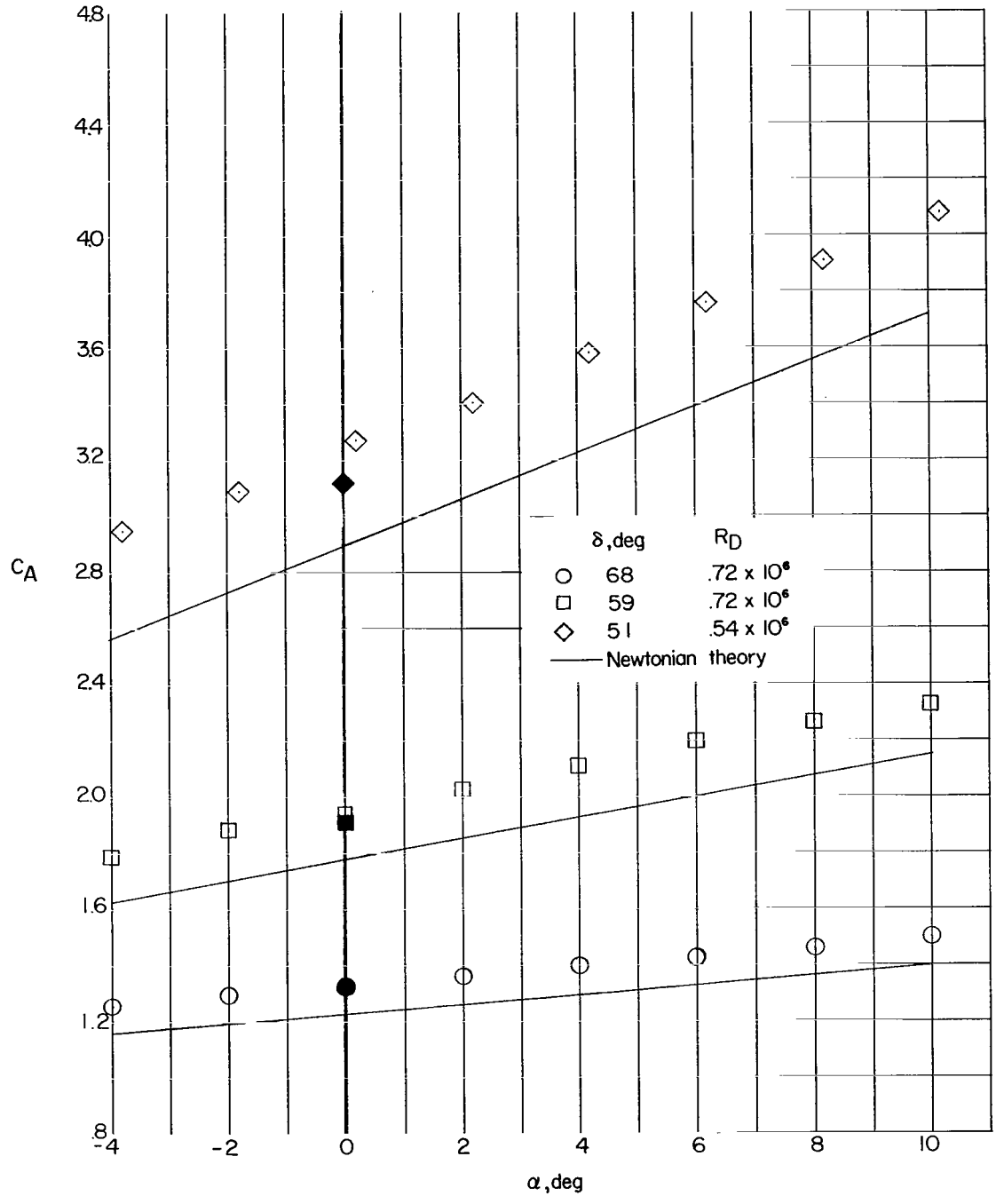

(b) Variation of C_A with α.

Figure 4.- Continued.

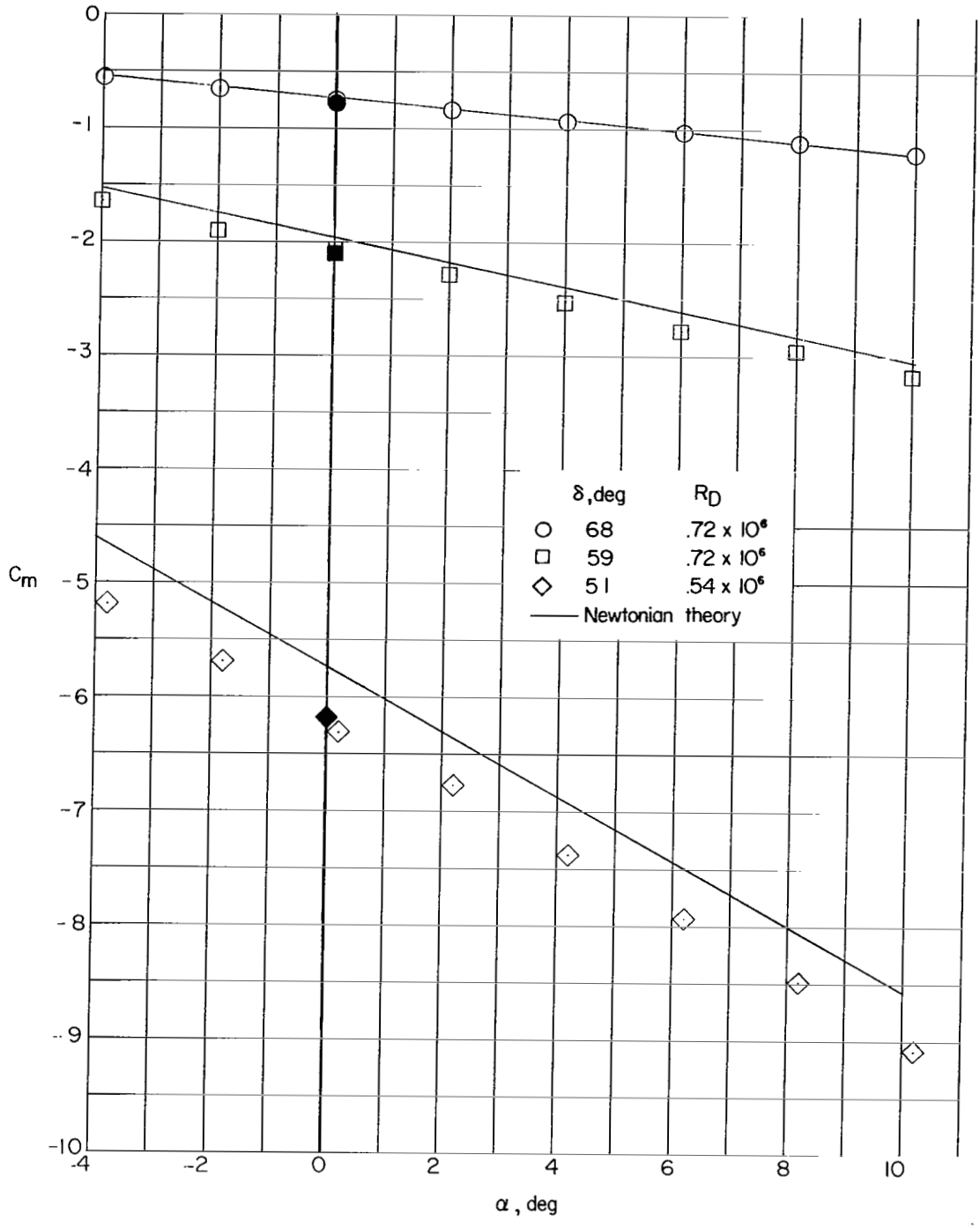

(c) Variation of C_m with α.

Figure 4.- Continued.

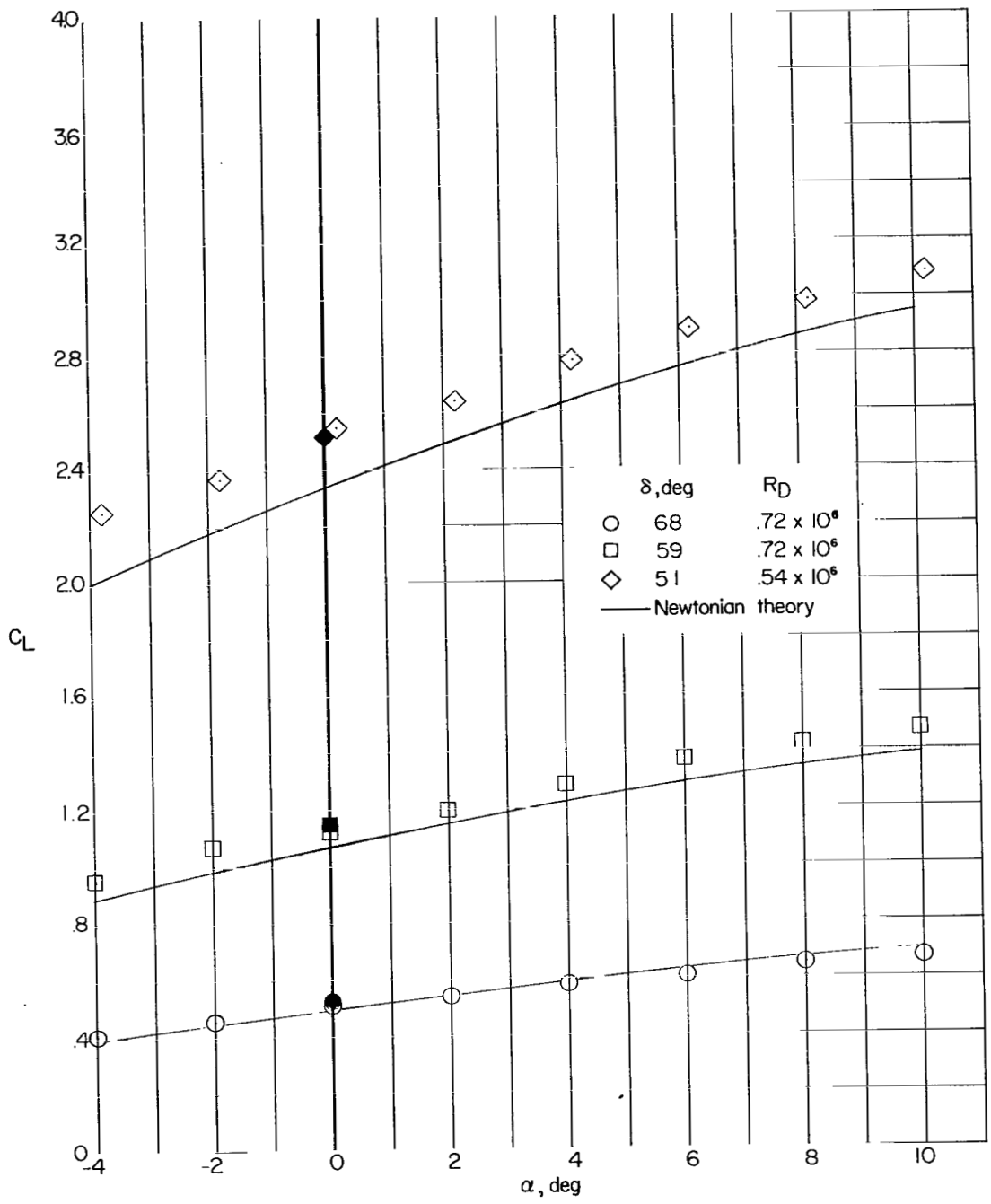

(d) Variation of C_L with α.

Figure 4.- Continued.

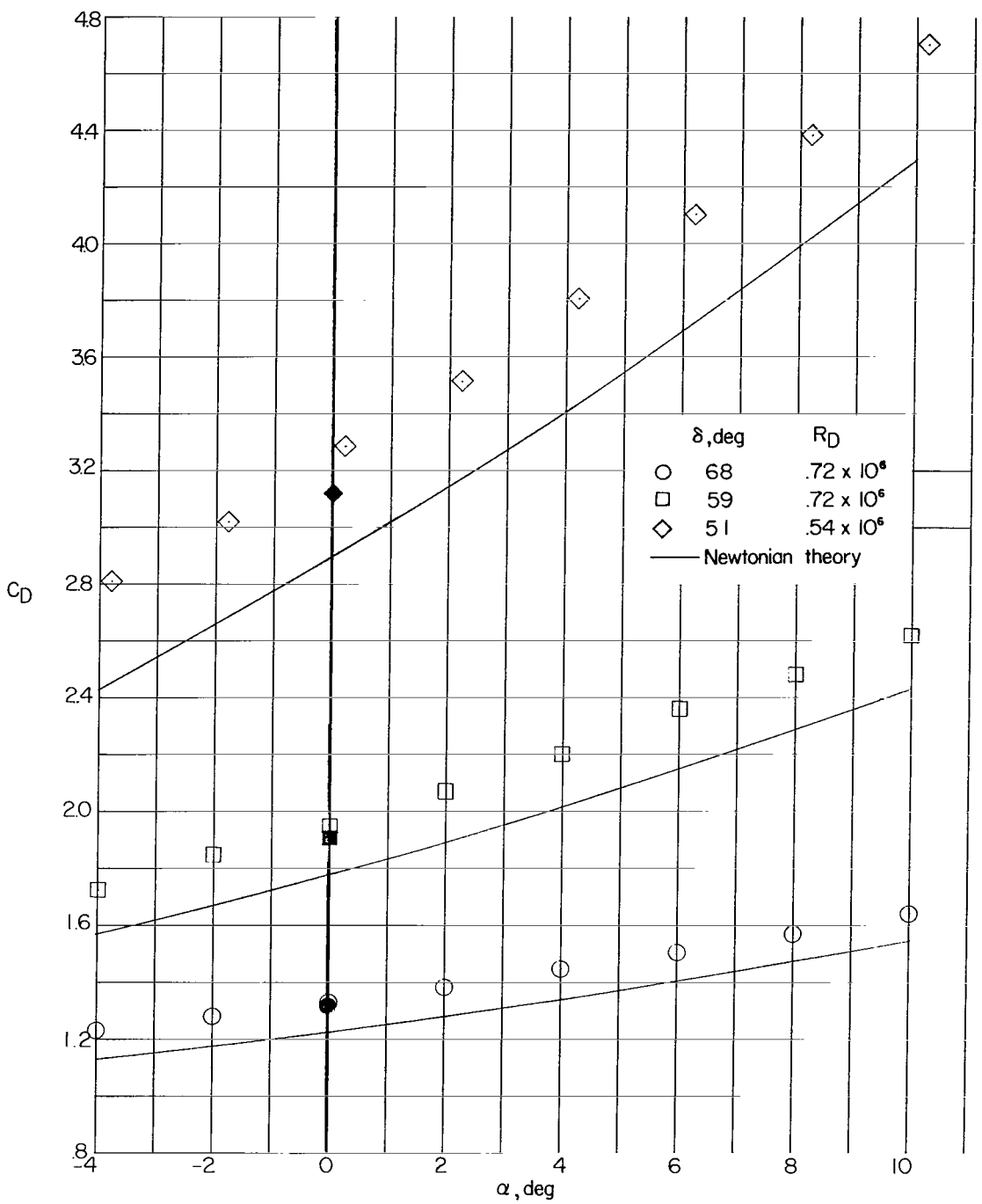

(e) Variation of C_D with α.

Figure 4.- Continued.

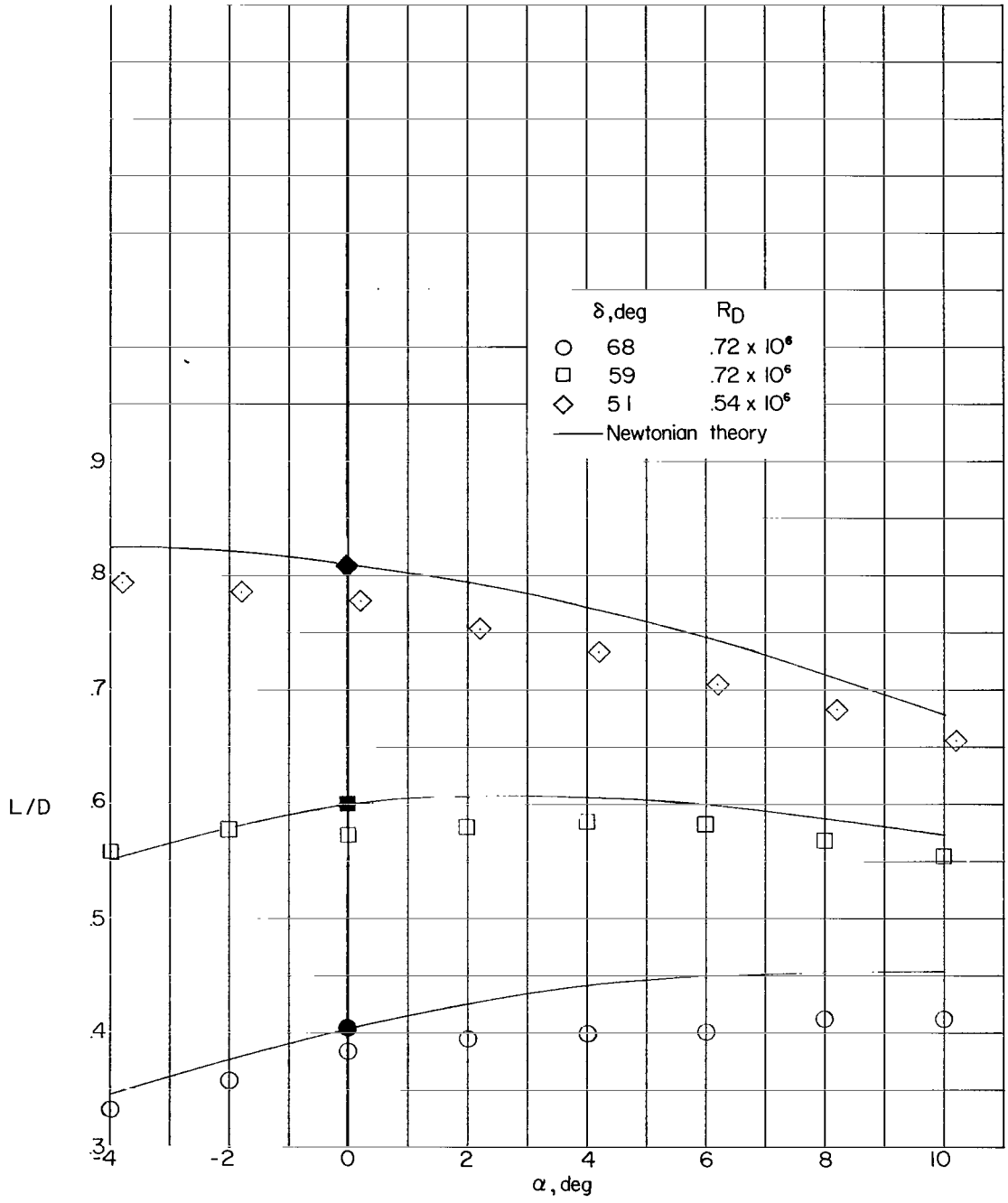

(f) Variation of L/D with α.

Figure 4.- Concluded.

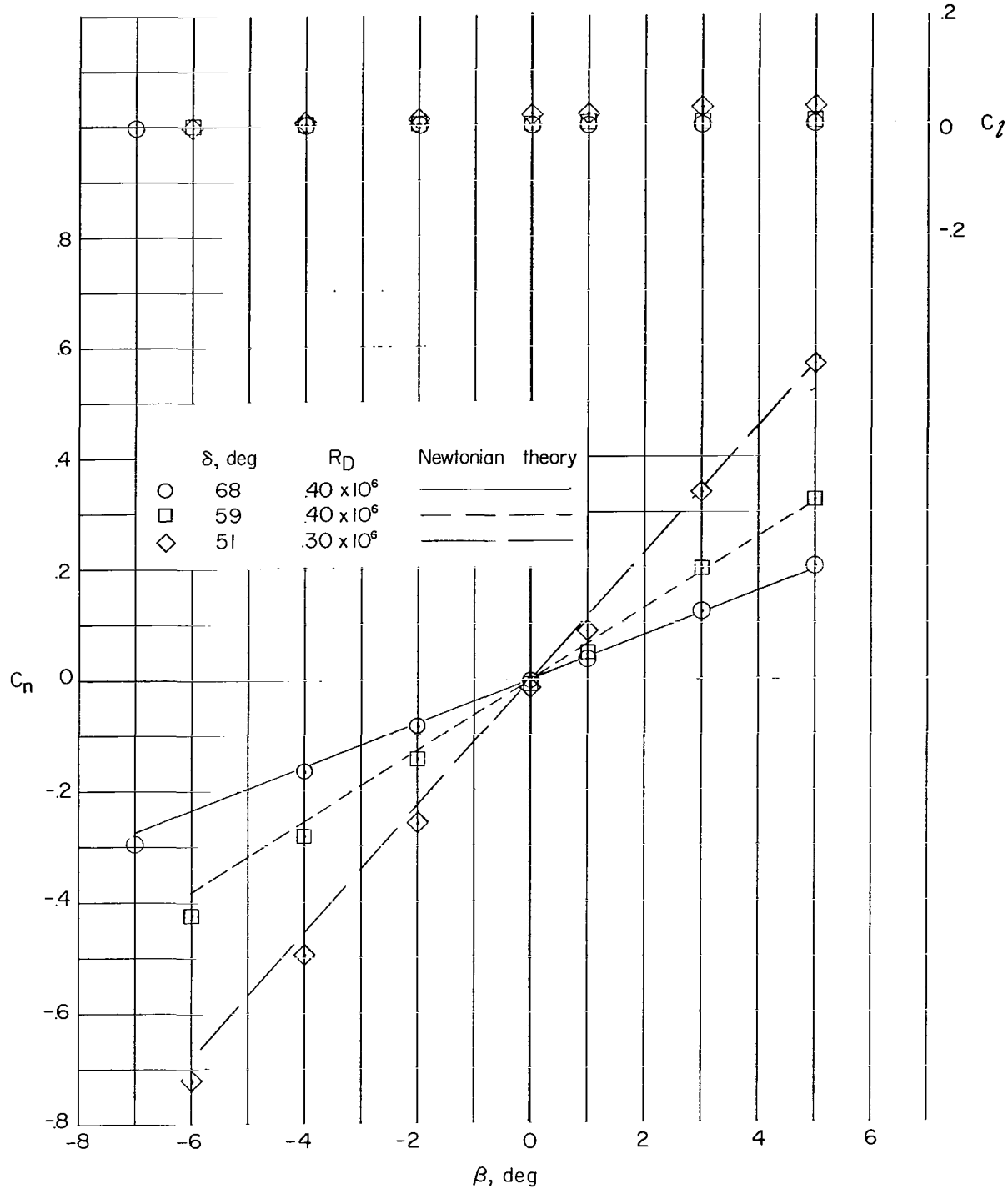

(a) Variation of C_n and C_l with β.

Figure 5.- Effect of rake-off angle on the lateral directional characteristics of circular cones at $\alpha = 0^0$. $\theta = 35^0$; $M_\infty = 19.1$.

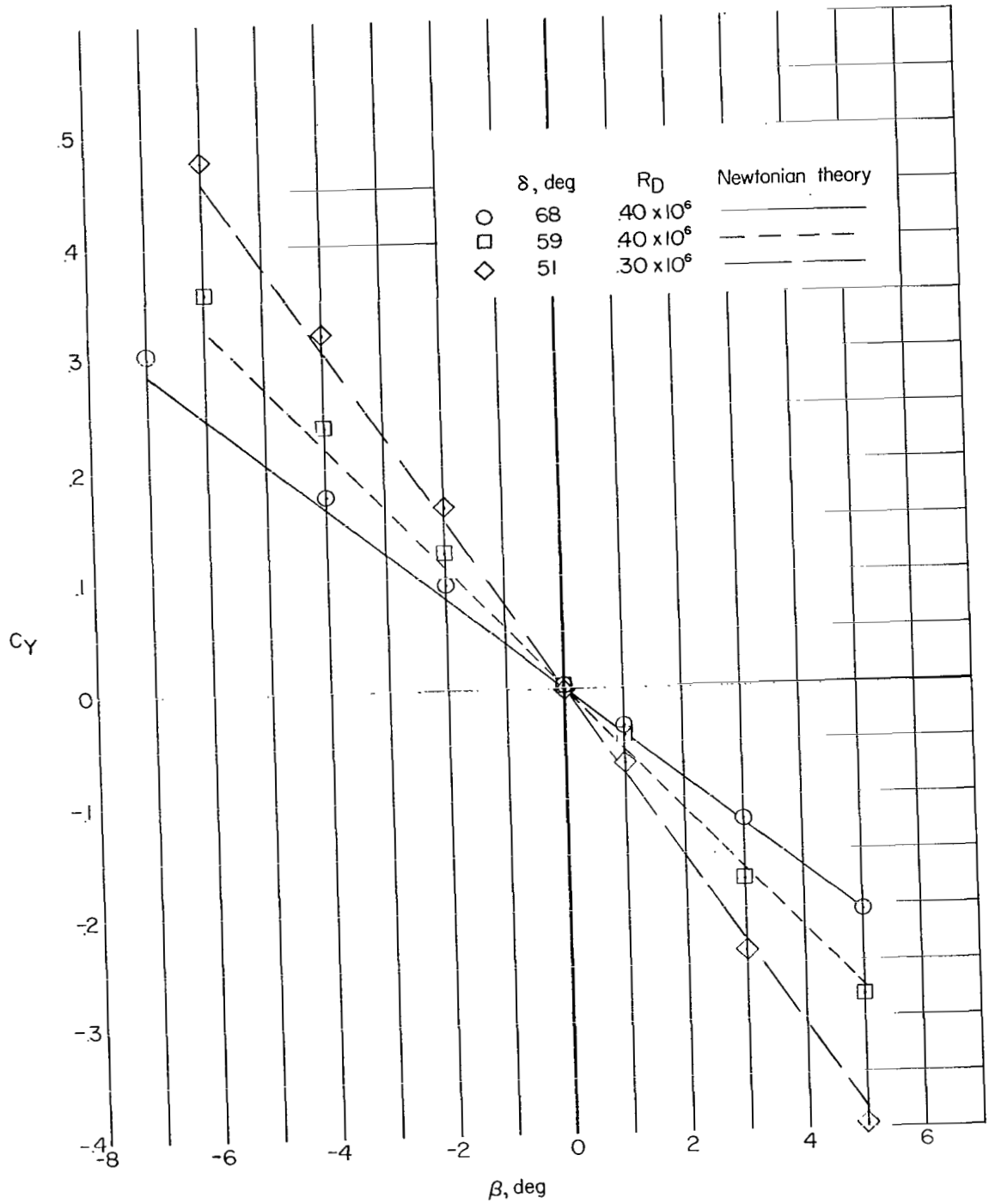

(b) Variation of C_Y with β.

Figure 5.- Concluded.

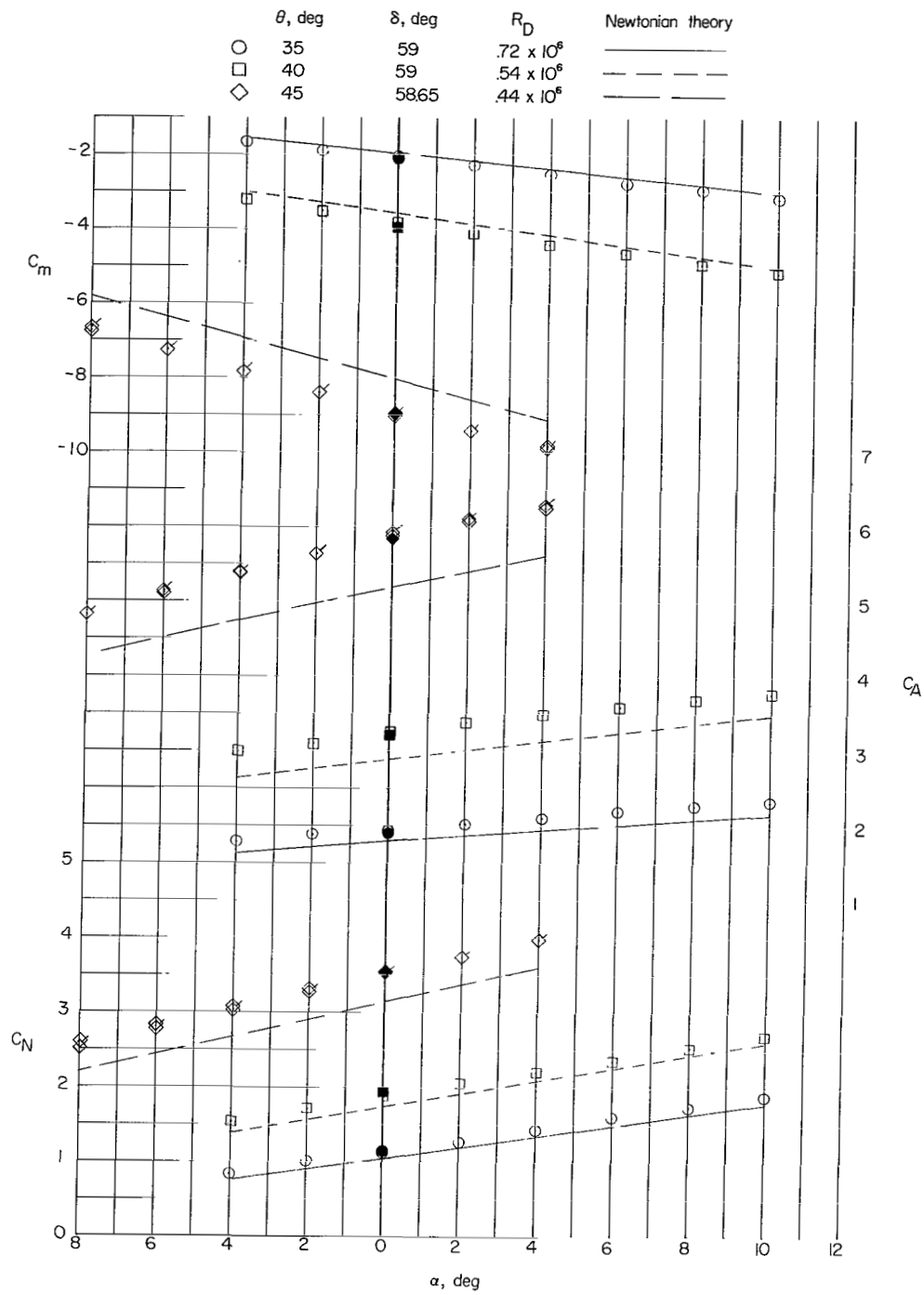

(a) Variation of C_N, C_A, and C_m with α.

Figure 6.- Effect of cone angle on the longitudinal characteristics of raked-off circular cones. $M_\infty = 20.2$. Solid symbols represent exact cone solution; flagged symbols represent configuration with afterbody.

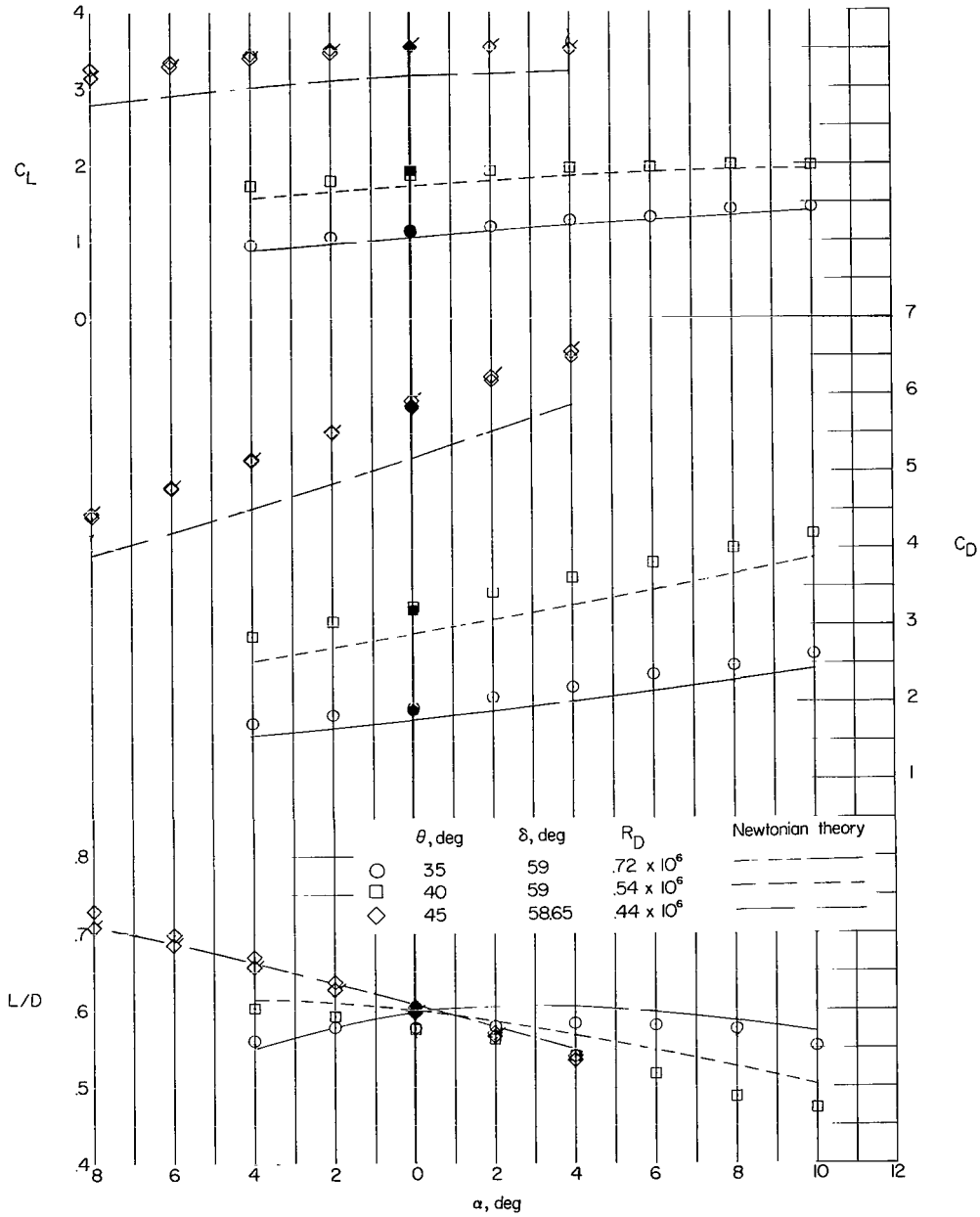

(b) Variation of C_L, C_D, and L/D with α.

Figure 6.- Concluded.

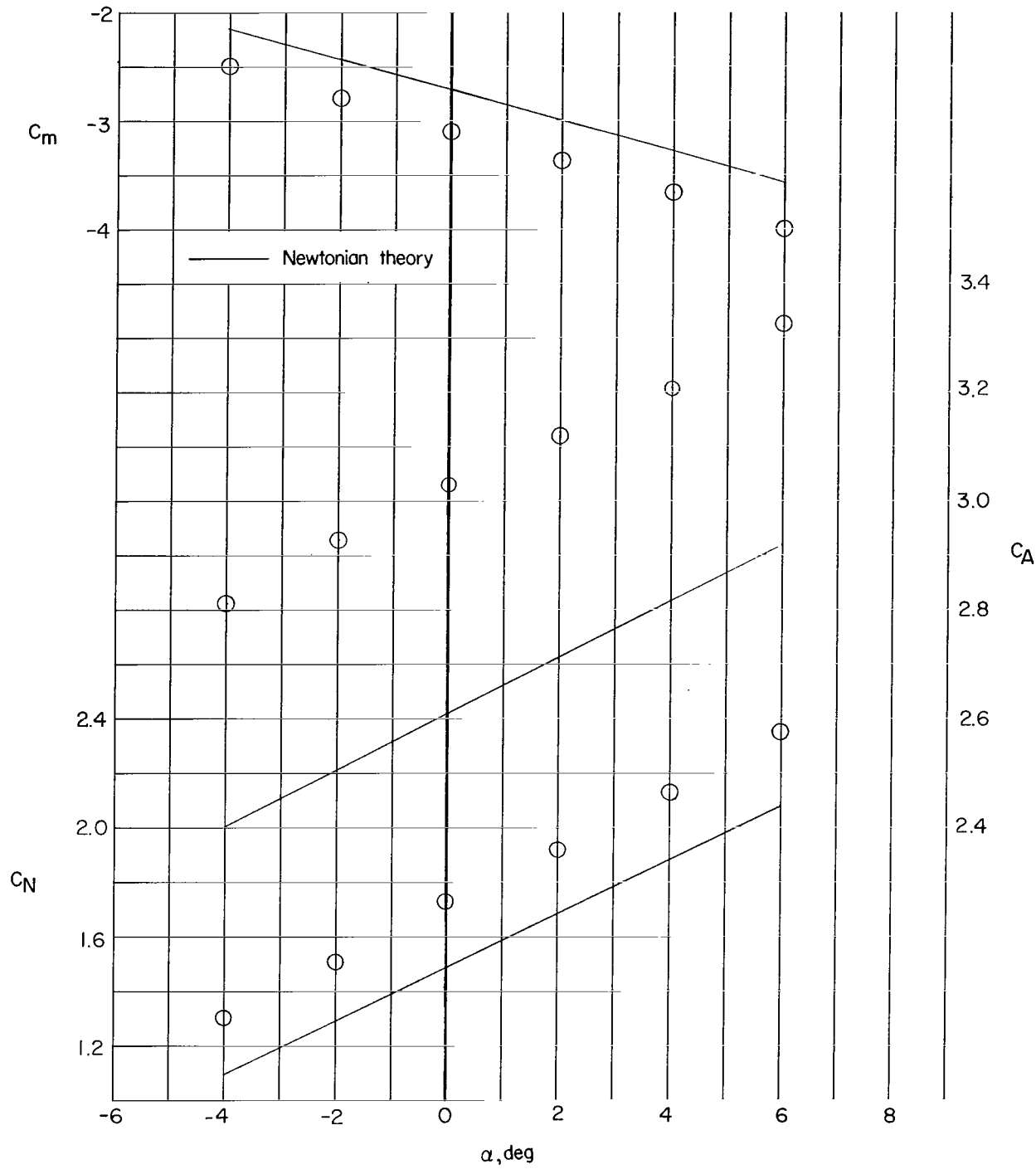

(a) Variation of C_N, C_A, and C_m with α.

Figure 7.- Aerodynamic characteristics of a raked-off elliptical cone. $M_\infty = 19.1$; $R_D = 0.40 \times 10^6$; $\theta_{XZ} = 35^0$; $\theta_{XY} = 42^0$; $\delta = 59^0$.

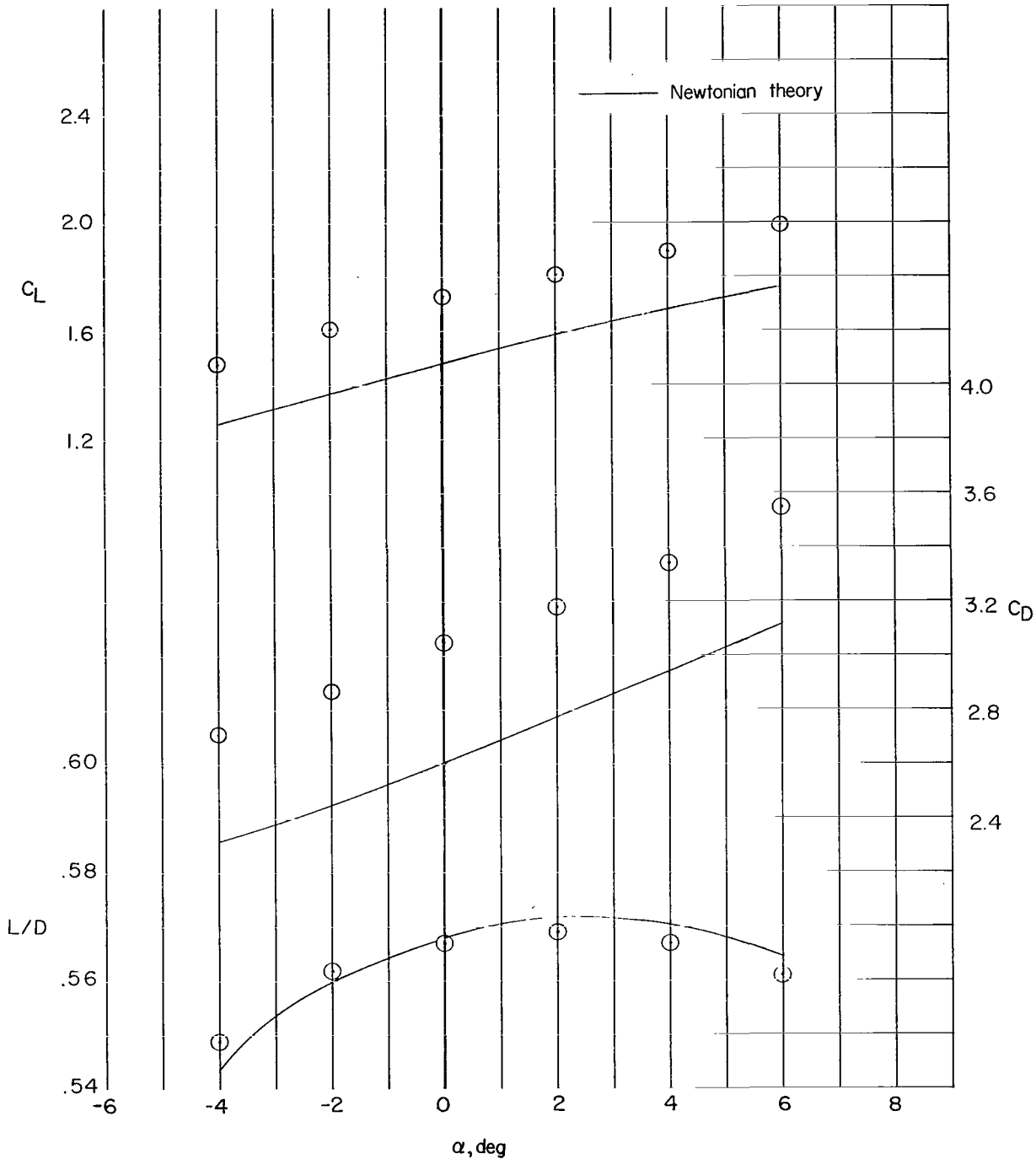

(b) Variation of C_L, C_D, and L/D with α.

Figure 7.- Continued.

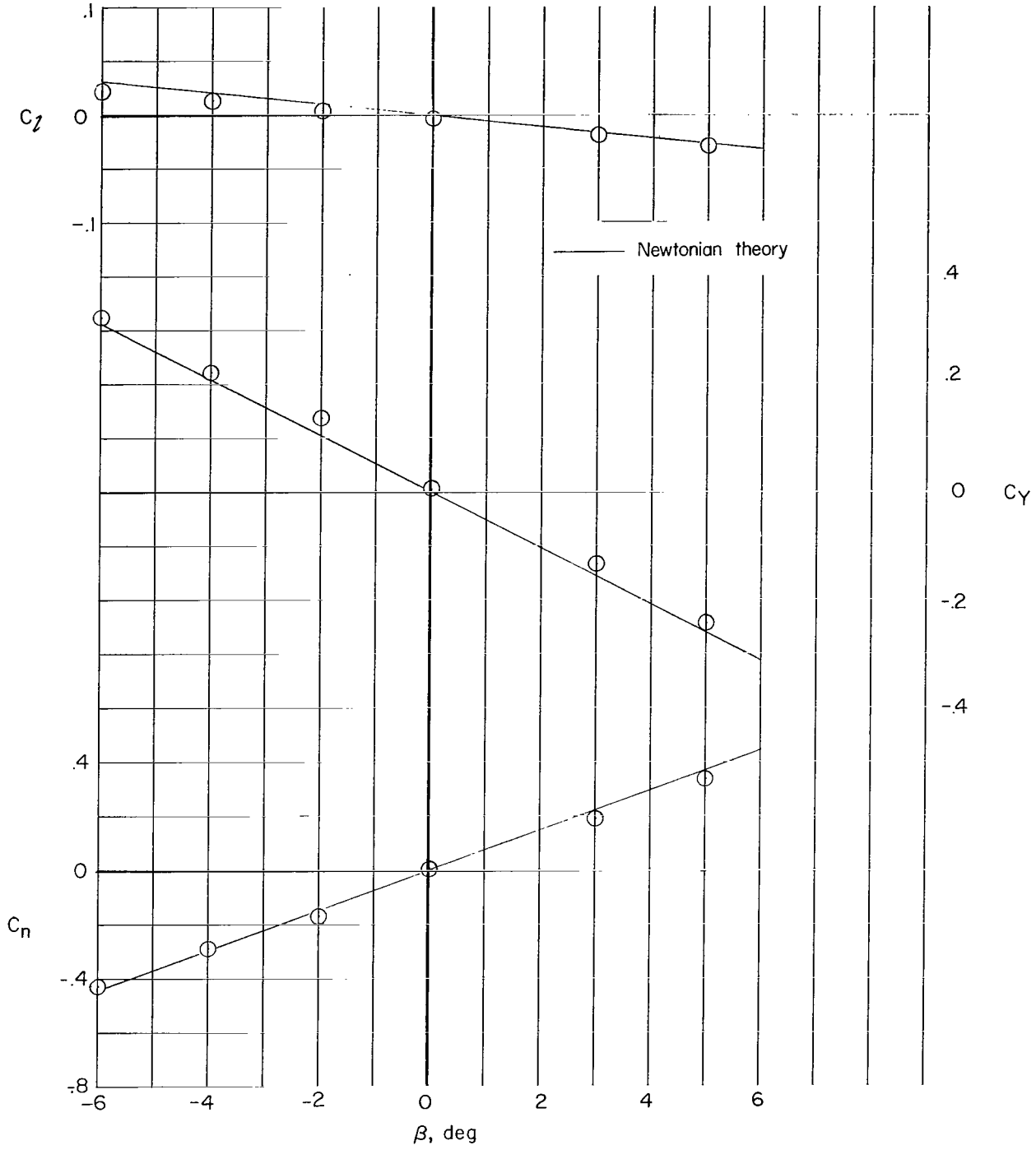

(c) Variation of C_n, C_Y, and C_l with β. $\alpha = 0^0$.

Figure 7.- Concluded.

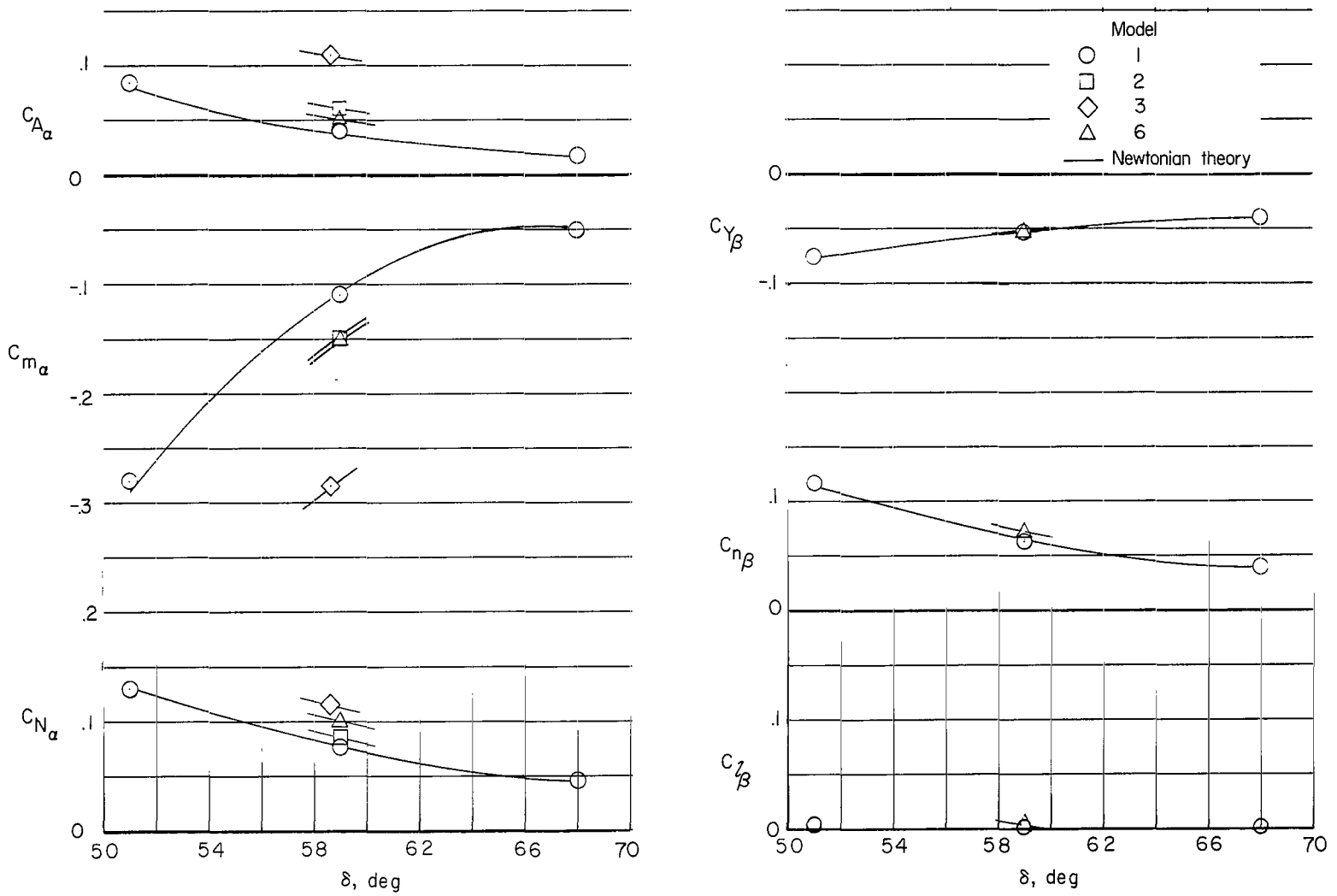

Figure 8.- Summary of stability derivatives at $\alpha = 0^0$.

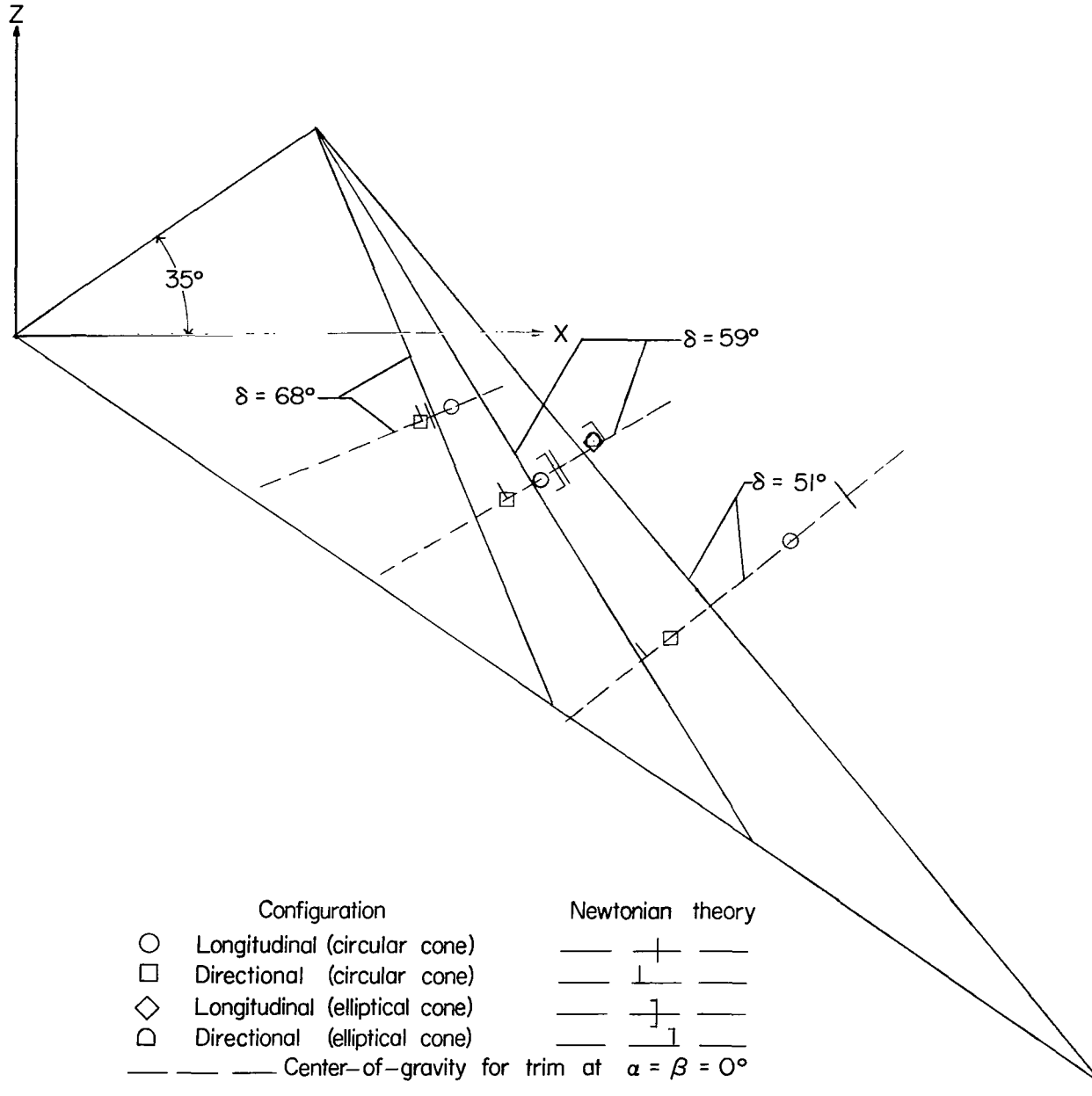

(a) $\theta_{XZ} = 35^0$.

Figure 9.- Limiting center-of-gravity locations for trimmed static stability.

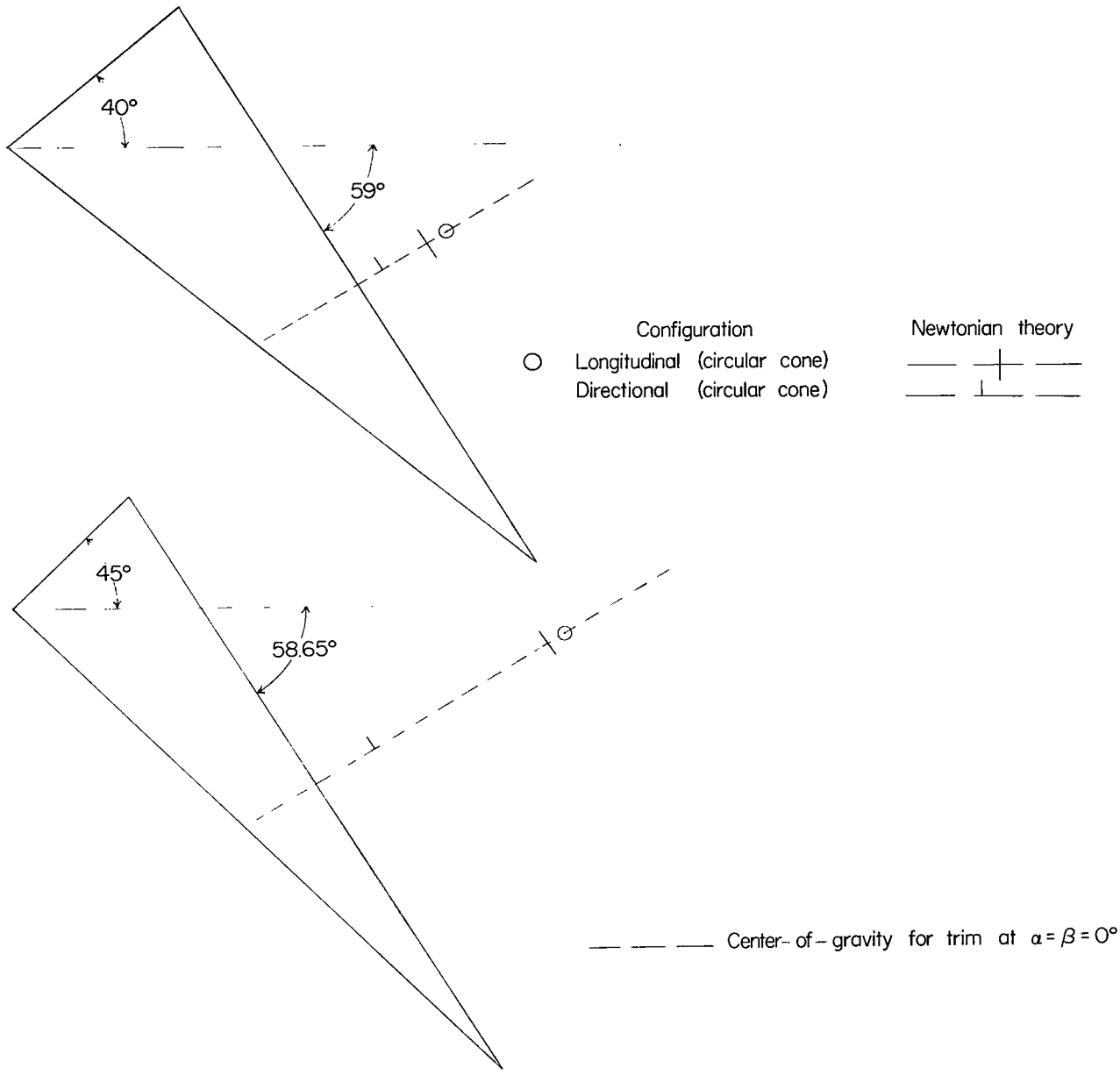

(b) $\theta_{XZ} = 40^0$ and 45^0.

Figure 9.- Concluded.

"The aeronautical and space activities of the United States shall be conducted so as to contribute . . . to the expansion of human knowledge of phenomena in the atmosphere and space. The Administration shall provide for the widest practicable and appropriate dissemination of information concerning its activities and the results thereof."

—NATIONAL AERONAUTICS AND SPACE ACT OF 1958

NASA SCIENTIFIC AND TECHNICAL PUBLICATIONS

TECHNICAL REPORTS: Scientific and technical information considered important, complete, and a lasting contribution to existing knowledge.

TECHNICAL NOTES: Information less broad in scope but nevertheless of importance as a contribution to existing knowledge.

TECHNICAL MEMORANDUMS: Information receiving limited distribution because of preliminary data, security classification, or other reasons.

CONTRACTOR REPORTS: Technical information generated in connection with a NASA contract or grant and released under NASA auspices.

TECHNICAL TRANSLATIONS: Information published in a foreign language considered to merit NASA distribution in English.

TECHNICAL REPRINTS: Information derived from NASA activities and initially published in the form of journal articles.

SPECIAL PUBLICATIONS: Information derived from or of value to NASA activities but not necessarily reporting the results of individual NASA-programmed scientific efforts. Publications include conference proceedings, monographs, data compilations, handbooks, sourcebooks, and special bibliographies.

Details on the availability of these publications may be obtained from:

SCIENTIFIC AND TECHNICAL INFORMATION DIVISION

NATIONAL AERONAUTICS AND SPACE ADMINISTRATION

Washington, D.C. 20546